THE JOURNAL OF BIOLOGICAL CHEMISTRY VOL. 282, NO. 43, pp. 31444–31452, October 26, 2007

The Structure of Human 4F2hc Ectodomain Provides a Model for Homodimerization and Electrostatic Interaction with Plasma Membrane*[S]

Received for publication, June 1, 2007, and in revised form, July 26, 2007 Published, JBC Papers in Press, August 26, 2007, DOI 10.1074/jbc.M704524200

Joana Fort[‡§1], Laura R. de la Ballina[‡1], Hans E. Burghardt[‡], Carles Ferrer-Costa[¶], Javier Turnay[‖], Cristina Ferrer-Orta[§], Isabel Usón[**], Antonio Zorzano[‡], Juan Fernández-Recio[¶‡‡], Modesto Orozco[¶], María Antonia Lizarbe[‖], Ignacio Fita[§2], and Manuel Palacín[‡3]

*From the [‡]Institute for Research in Biomedicine, Barcelona Science Park and the Department of Biochemistry and Molecular Biology, Faculty of Biology, University of Barcelona and Centro de Investigación Biomédica en Red de Enfermedades Raras, E-08028 Barcelona, the [§]Instituto de Biología Molecular de Barcelona (Consejo Superior de Investigaciones Científicas), Institute for Research in Biomedicine, Barcelona Science Park, Barcelona E-08028, [¶]Molecular Modeling and Bioinformatics, Institute for Research in Biomedicine, Barcelona E-08028, the [‖]Departamento de Bioquímica y Biología Molecular I, Facultad de Ciencias Químicas, Universidad Complutense, E-28040 Madrid, **ICREA at Instituto de Biología Molecular de Barcelona (Consejo Superior de Investigaciones Científicas), E-08028 Barcelona , and [‡‡]Barcelona Supercomputing Center, E-08028 Barcelona, Spain*

4F2hc (CD98hc) is a multifunctional type II membrane glycoprotein involved in amino acid transport and cell fusion, adhesion, and transformation. The structure of the ectodomain of human 4F2hc has been solved using monoclinic (Protein Data Bank code 2DH2) and orthorhombic (Protein Data Bank code 2DH3) crystal forms at 2.1 and 2.8 Å, respectively. It is composed of a $(\beta\alpha)_8$ barrel and an antiparallel β_8 sandwich related to bacterial α-glycosidases, although lacking key catalytic residues and consequently catalytic activity. 2DH3 is a dimer with Zn^{2+} coordination at the interface. Human 4F2hc expressed in several cell types resulted in cell surface and Cys^{109} disulfide bridge-linked homodimers with major architectural features of the crystal dimer, as demonstrated by cross-linking experiments. 4F2hc has no significant hydrophobic patches at the surface. Monomer and homodimer have a polarized charged surface. The N terminus of the solved structure, including the position of Cys^{109} residue located four residues apart from the transmembrane domain, is adjacent to the positive face of the ectodomain. This location of the N terminus and the Cys^{109}-intervening disulfide bridge imposes space restrictions sufficient to support a model for electrostatic interaction of the 4F2hc ectodomain with membrane phospholipids. These results provide the first crystal structure of heteromeric amino acid transporters and suggest a dynamic interaction of the 4F2hc ectodomain with the plasma membrane.

4F2hc (CD98hc, FRP-1, and SLC3A2) is a multifunctional type II membrane glycoprotein involved in amino acid transport (1), cell fusion (2), and β1 integrin-dependent adhesion (3). 4F2hc and the homologous rBAT are the heavy subunits of the heteromeric amino acid transporters (HATs),[4] which are linked by a disulfide bridge to the catalytic light subunit (Fig. 1*A*). One of six light subunits (LAT1, LAT2, y^+LAT1, y^+LAT2, asc-1, and xCT) heterodimerizes with 4F2hc, thereby rendering a range of transport activities. 4F2hc-associated light subunits are involved in human pathology (y+LAT1 mutations cause lysinuric protein intolerance, and xCT is the receptor of Kaposi sarcoma-associated herpesvirus (4–6)). The known role of the heavy subunits is to bring the holotransporter to the plasma membrane. Moreover, 4F2hc is involved in cellular transformation because it is highly expressed in tumor cells; its expression correlates with tumor development, progression, and metastatic potential; and its overexpression leads to cell transformation (7–10). 4F2hc is a mediator of β1 integrin signaling (11). Recently, a metabolic activation-related CD147-4F2 complex has been identified on the cell surface that may play a critical role in energy metabolism, probably by coordinating the transport of lactate (via MCT1 and MCT4) and amino acids (via LAT1) (12). Integrin interaction and the CD147-4F2 complex may explain the role of 4F2hc in cellular transformation.

The role of the big ectodomain of the heavy subunits of HATs remains largely unknown. The 4F2hc ectodomain (4F2hc-ED) is required for plasma membrane localization of the light subunits LAT2 and y^+LAT2 (13). 4F2hc-ED might also modulate β1 integrin function and tumorigenicity (10), although interactions with β1 integrins involve the transmembrane and the

* This work was supported in part by the Spanish Ministry of Science and Education Grant SAF2003-08940, BFU2006-14600, and BIO2005-06753, by the EC Project Grant 502802 EUGINDAT, and by La Marató-TV3. The costs of publication of this article were defrayed in part by the payment of page charges. This article must therefore be hereby marked "*advertisement*" in accordance with 18 U.S.C. Section 1734 solely to indicate this fact.

The atomic coordinates and structure factors (code 2DH2 and 2DH3) have been deposited in the Protein Data Bank, Research Collaboratory for Structural Bioinformatics, Rutgers University, New Brunswick, NJ (http://www.rcsb.org/).

[S] The on-line version of this article (available at http://www.jbc.org) contains supplemental Materials and Methods, additional references, Figs. 1–8, and Table 1.

[1] Both authors should be considered first authors. Recipients of a predoctoral fellowship from the Spanish Ministry of Science and Education.

[2] To whom correspondence may be addressed. Tel.: 34-934034949; E-mail: ifrcri@ibmb.csic.es.

[3] To whom correspondence may be addressed. Tel.: 34-934037199; E-mail: mpalacin@pcb.ub.es.

[4] The abbreviations used are: HAT, heteromeric amino acid transporter; PDB, Protein Data Bank; HA, hemagglutinin; DTT, dithiothreitol; NTA, nitrilotriacetic acid; ER, endoplasmic reticulum; Endo, endo-β-*N*-acetylglucosaminidase; PBS, phosphate-buffered saline.

N-terminal intracellular segments of 4F2hc (14). Recently, interaction of galectin-3 with 4F2hc-ED has been reported to play a role in trophoblast formation by cell fusion in the placenta (15).

Intriguingly, the ectodomains of the heavy subunits of HATs show homology with α-amylases (glycosyl hydrolase family 13 members) (16). The low amino acid sequence identity of the C-terminal half of 4F2hc-ED with α-amylases precluded the generation of a reliable three-dimensional model by homology (1). The crystal structure of 4F2hc-ED solved here supports an electrostatic interaction of the ectodomain with the plasma membrane and suggests a receptor function for the α-amylase-like cleft. The crystal structure also evidences a tendency of 4F2hc to form homodimers, which has been confirmed in cell expression studies.

MATERIALS AND METHODS

Production of Human 4F2hc-ED in Escherichia coli—The cDNA sequence coding the 4F2hc-ED (residues 111–530 of human 4F2hc) was digested from the pSPORT-4F2hc plasmid (17) with NruI and HindIII. The insert was cloned into the pTrcHisA vector (Invitrogen), previously digested with BamHI, and then treated with Klenow and digested with HindIII. The resulting plasmid was transformed into BL21 (DE3) cells (Novagen), and the cells were grown in LB media at 37 °C. Cells with $A_{600} = 0.6$ were induced with 1 mM isopropyl 1-thio-β-D-galactopyranoside followed by culture for 16 h at 37 °C. Harvested cells were resuspended in lysis buffer (20 mM potassium phosphate, pH 8.0, 500 mM NaCl, 1 mg/ml lysozyme (Roche Applied Science), 5 μg/ml DNase (Roche Applied Science), 1 mM phenylmethylsulfonyl fluoride, aprotinin, pepstatin, and leupeptin) and lysed on a French press at 20,000 p.s.i. The resulting cell lysate was centrifuged twice at 16,000 × *g* for 45 min. The soluble fraction was applied to a HiTrap chelating 5-ml column (Amersham Biosciences), previously charged with Ni^{2+}, in an Ákta-FPLC. The buffer was changed to 50 mM Tris, 1 mM $CaCl_2$,0.1% Tween 20, and 4F2hc-ED was eluted by overnight digestion with enterokinase (50 units/column) (Invitrogen). Furthermore, it was purified by MonoQ chromatography, and the final yield was 2 mg of 4F2hc-ED/liter of initial culture. Protein was concentrated with centrifugal filters (Amicon Ultra 15 10,000 Da, Millipore) to ~15 mg/ml for crystallization. Circular dichroism was used to control the quality of the protein samples used in the crystallization trials. The percentage of secondary structure of 4F2hc-ED derived in solution was in agreement with the crystal structure (data not shown). A similar approach to produce human rBAT-ED was unsuccessful because of the low protein production and the incorporation into inclusion bodies (data not shown).

Crystallization and Data Collection—Two types of 4F2hc-ED crystals, needles and plates, were obtained by the hanging drop vapor diffusion method at 20 °C. Needles were monoclinic (space group $P2_1$) and grew in 25% PEG 4000, 0.2 M sodium acetate, and 0.1 M Tris buffer, pH 8.5. Plates were orthorhombic (space group $P2_12_12_1$) and grew in 25% PEG 3350, 0.2 M ammonium sulfate, measured pH ~6. Crystals were flash-cooled in the presence of 10% glycerol for the monoclinic crystal and 30% PEG 4000 1 M KI for the orthorhombic crystal. X-ray diffraction data were collected at beamline ID13 at the ESFR (Grenoble, France) with a MarCCD detector at 100 K. Data were processed and scaled using the DENZO and SCALEPACK programs, respectively (Table 1).

Structure Determination and Refinement—Molecular replacement searches on the monoclinic crystals, which contain one 4F2hc-ED molecule in their asymmetric unit, were performed following the CaspR protocols (CaspR server; CNRS, Marseille, France) (18) starting with three PDB structures of prokaryotic α-glycosidases (PDB codes 1JI2, 1SMA, and 1UOK), which had sequence identities of about 25% with respect to 4F2hc-ED. The TIM-barrel domain fragment from the best refined solution was then fixed, and the C-terminal domain was reoriented using MOLREP (19). The new polyalanine structure was further modified by rigid body refinement with Refmac5 (20) of different fragments. The resulting model allowed us to obtain an initial solution, with AMoRe (21), for the orthorhombic crystal, which contains two 4F2hc-ED molecules in the asymmetric unit. Electron density was improved by averaging between the two crystal forms with *DMMULTI* (22). Model rebuilding and refinement was completed, for the two crystal forms, by iterative cycles of manual and automatic refinement with the graphic programs O (23) and Refmac5, respectively (Table 1). The stereochemistry of the models was checked with PROCHECK (24). The programs T-Coffee and ESPript were used for sequence and structural alignments and their representation, respectively (25, 26). Cavities were analyzed with the CASTp plug-in (27). Electrostatic surfaces were computed with GRASP (28). All structure pictures were drawn with PyMol (29).

Co-precipitation of 4F2hc-HA and His-4F2hc—HeLa cells were transiently co-transfected with combinations of wild-type human 4F2hc-HA, C109S 4F2hc-HA, pCDNA3.1, and wild-type human His-4F2hc (see supplemental Materials and Methods). Two days later, cells were lysed with 400 μl/10-cm plate of lysis solution (0.3 M NaCl, 1% Triton X-100, 0.025 M imidazole, protease inhibitor mixture (1 mM phenylmethylsulfonyl fluoride, 1 units/ml aprotinin, 1 μM leupeptin and 1 μM pepstatin), and 0.05 M $NaPO_4$, pH 7.4). Cells were then scraped, transferred into a 1.5-ml tube, and incubated on a rotating orbital shaker at 4 °C. After 1 h, the insoluble material was removed by centrifugation at 12,000 rpm for 10 min. Supernatants were incubated with 20 μl of Ni-NTA-agarose beads (Qiagen) previously equilibrated with 150 μl of lysis solution for 30 min at 4 °C. After 1.5 h of incubation at 4 °C with the solubilized cellular proteins, beads were washed twice in 750 μl of a PBS solution containing 0.5 M NaCl and 0.05 M imidazole, pH 7.4. Proteins were eluted by 15 min of shaking incubation at 25 °C with 45 μl of elution buffer (PBS containing 0.5 M NaCl and 0.25 M imidazole, pH 7.4). 4-Fold concentrated Laemmli Sample Buffer was added to the eluates from the Ni-NTA beads.

Cross-linking—Intact cells overexpressing different forms of 4F2hc-HA were grown to 90% confluence in 10-cm plates and then washed two times with PBS, pH 7.0. Cross-linker $BM[PEO]_2$ (Pierce) (1 mM in PBS pH 7.0) was added for 1 h of incubation at room temperature before termination with 50 mM dithiothreitol (DTT). After washing with PBS, cells were homogenized in lysis buffer (PBS, 1% Triton X-100, and the

same protease inhibitor mixture as above) at 4 °C for 1 h. Lysates were centrifuged at 13,000 × *g* for 5 min, and supernatants were processed for Western blot analysis in the presence of DTT (100 μM).

Endo H and Endo F Treatments—Total protein extracted as in the previous section (cross-linking) from HeLa cells (1 mg/ml) were treated with Glycoprotein Denaturing Buffer and incubated at 99 °C for 10 min. Reaction mixtures for Endo $H_{.F.}$ (30 units/μl in G5 buffer) and peptide:*N*-glycosidase F (30 units/μl in G7 buffer with 1% Nonidet P-40) treatments were incubated at 37 °C for 1 h. Controls were performed with water instead of enzyme. In cases where reactions were carried out in nonreducing conditions, the Glycoprotein Denaturing Buffer was substituted by 0.5% SDS. All reagents and buffers were from New England Biolabs.

Western Blot Analysis—Protein extracts, obtained as above, from different origins in Laemmli Sample Buffer containing or not 100 mM DTT were loaded for SDS-PAGE (7.5% polyacrylamide). c-Myc, HA, and His tags were detected with antibodies sc-789 (1:500; Santa Cruz Biotechnology), 3F10 (1:1000; Roche Applied Science), and anti-HisG (1:5000; Invitrogen), respectively.

Computational Analysis—For molecular dynamics simulations, the monomeric crystal structure was fully solvated with an octahedron tip3p water box; ions were added, and final system was minimized and equilibrated to 300 K using amber force field (30) in namd program (31, 32). Finally, 10 ns of production were collected and analyzed as described (33). Optimal desolvation area calculations were performed by using a variation of the described protocol, defining the optimal patches from the center of coordinates of every residue side chain instead of from a series of surface points as in the original method (34). Protein-protein docking calculations were performed by the pyDock protocol, as recently described (35). We used FTDOCK (36) to generate 10,000 rigid-body docking orientations, which were evaluated by the pyDock scoring function optimized for rigid-body docking. The resulting orientations were further clustered by in-house software. Briefly, for each docking solution, the rotation matrix and translation vector were converted to the rotation axis, rotation angle, and translation vector that relate ligand and receptor coordinates. The combined three angular measures defined a distance between solutions that was used in an in-house implementation of a standard clustering method. Symmetry and filter distances (<17 Å between the two homologous S444C and S480C residues for cross-linking experiments and distance <30 Å between the two homologous residues Gln^{115} for disulfide bridge formation (residues previous to Gln^{115} were not included in the docking calculations because of their mobility)) were also applied using in-house software.

RESULTS

Overall Structure of Human 4F2hc-ED—We built a 4F2hc-ED construct that included the human 4F2hc residues from Glu^{111} to the C-terminal Ala^{529}, plus a six-residue N-terminal extension (Lys-Asp-Arg-Trp-Gly-Ser) corresponding to the expression plasmid. The construct was crystallized in both a monoclinic ($P2_1$) and an orthorhombic ($P2_12_12_1$) crystal form.

TABLE 1
Data collection and refinement statistics (molecular replacement)

	PDB code 2DH2	PDB code 2DH3
Data collection		
Space group	$P2_1$	$P2_12_12_1$
Cell dimensions		
a, *b*, *c* (Å)	39.7, 67.8, 74.0	69.5, 101.8, 122.0
α, β, γ (°)	90.0, 98.5, 90.0	90.0, 90.0, 90.0
Resolution (Å)	25.0-2.1 (2.2-2.1)[a]	30.0-2.8 (2.9-2.8)
R_{sym}	8.4 (54.9)	5.7 (27.0)
$I/\sigma I$	7.3 (1.5)	15.7 (3.5)
Completeness (%)	97.3 (98.8)	94.3 (96.2)
Redundancy	4.5 (2.9)	7.1 (4.2)
Refinement		
Resolution (Å)	19.8-2.10	29.6-2.8
No. of reflections	22,652	19,650
R_{work}/R_{free}	17.8/23.0	22.0/27.5
No. of atoms		
Protein	3,269	6,504
Ligand/ion	4 (acetate)	1 (zinc)
Water	139	28
B-factors		
Protein	34.0	51.1
Ligand/ion	44.3	46.0
Water	37.5	36.8
Root mean square deviations		
Bond lengths (Å)	0.012	0.006
Bond angles (°)	1.446	1.180
Ramachandran plot		
Residues in disallowed regions	1 (Ser^{480})	1 in chain A (Phe^{218}) 1 in chain B (Leu^{284})

[a] Values in parentheses are for the highest resolution shell.

Structure determination was achieved by molecular replacement and crystal averaging (see "Materials and Methods"). The final refined structures present crystallographic agreement factors *R* and R_{free} of 17.8/23.0 and 22.0/27.5 at resolutions of 2.1 and 2.8 Å for the monoclinic and orthorhombic crystals, respectively (Table 1). Structures include residues Gly^{109}–Ala^{529} for the subunit in the monoclinic crystal (PDB code 2DH2) and Ala^{114}–Ala^{529} and Gly^{109}–Ala^{529} for the two subunits in the orthorhombic crystal (PDB code 2DH3).

The structure of 4F2hc-ED can be described in terms of topology and multidomain organization of α-amylases (Fig. 1, *B* and *C*). In 4F2hc-ED, the so-called A-domain in α-amylases, a $(\beta/\alpha)_8$ TIM-barrel, corresponds to the N-terminal globular domain. This domain starts with two contiguous tryptophan residues (Trp^{117}–Trp^{118}) without insertions until Lys^{431}. A 6-residue-long helix (Arg^{433}–His^{438}) connects the A-domain to the C-terminal domain, which corresponds to the so-called C-domain, which, although presenting a variable β-sandwich topology, is always present in α-amylases. The C-domain of 4F2hc includes residues from Asp^{439} to the carboxyl end Ala^{529}. The interface between domains A and C is very hydrophobic, 67% of the total contact surface (2538 $Å^2$), and involves mainly the secondary structure elements Aα6 to Aα8 and Cβ1 to Cβ3. 4F2hc lacks a B-domain, a globular insertion between the third β-strand (Aβ3), and the third α-helix (Aα3) of the A-domain, which is present in many α-amylases. In the three independent crystallographic 4F2hc-ED structures determined, residues that precede Trp^{117} adopt an extended conformation pointing toward the interface between the A- and C-domains in the vicinity of Trp^{456}, a fully conserved residue in 4F2hc from vertebrates. Residue 109 in 4F2hc is a cysteine that makes a disulfide bridge with the light subunit and is just four residues away from the putative transmembrane segment. Our structure sug-

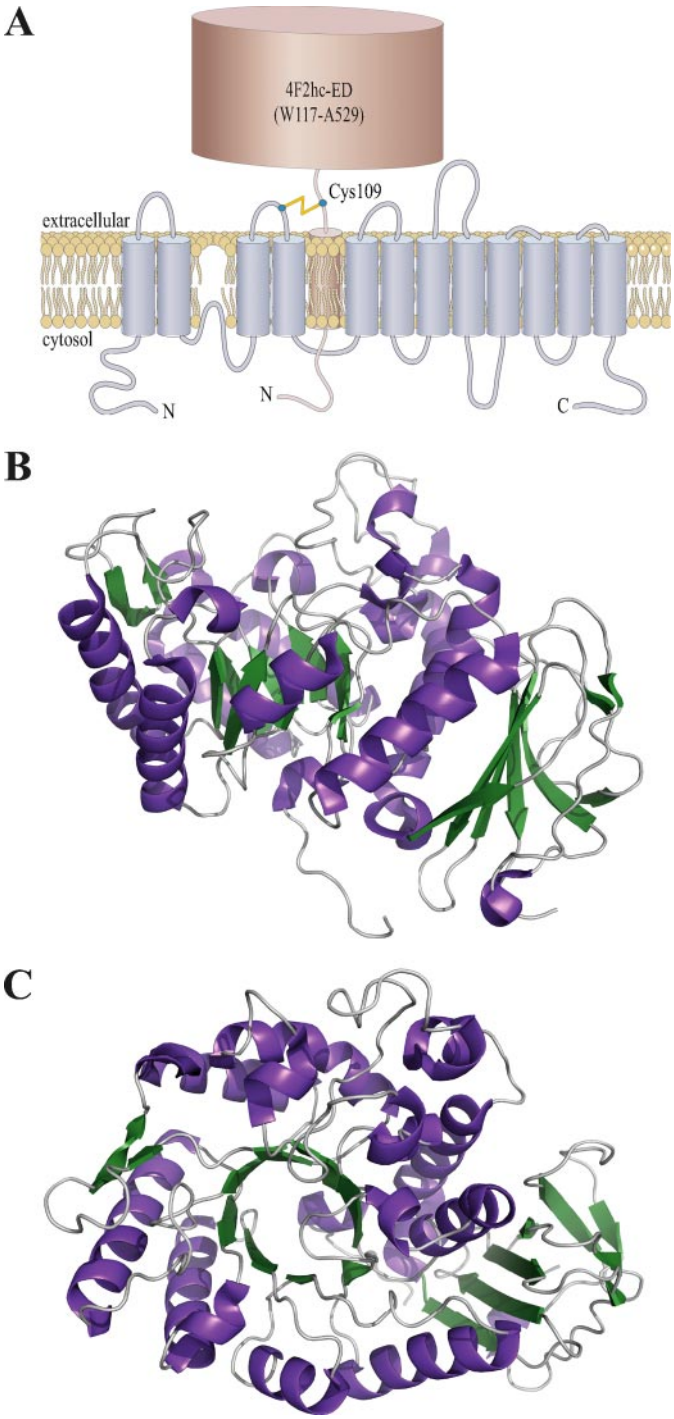

FIGURE 1. **Structure of 4F2hc-ED.** *A,* HAT schematic representation. 4F2hc (*pink*) with a bulky *N*-glycosylated ectodomain (4F2hc-ED, covering residues Trp^{117} to the C-terminal Ala^{529}) is linked by a conserved disulfide bridge (Cys^{109} in human 4F2hc) with a light subunit (*blue*), a 12 trans-membrane-spanning nonglycosylated protein. Lateral (*B*) and upper (*C*) views of 4F2hc-ED structure. The N-terminal position corresponds to Cys^{109}. The structure is similar to that of α-glycosidases, including two domains: a TIM-barrel $(\beta/\alpha)_8$ and a C-terminal domain with eight antiparallel β-sheets.

gests that the location of the N terminus imposes strong structural restrains with respect to both the docking of 4F2hc onto the membrane and the interactions with the light subunit in the heterodimer (Fig. 1*B*).

Human 4F2hc presents four putative *N*-glycosylation sites in the A-domain (Asn^{264} in Aα4, Asn^{280} just before Aα5, Asn^{323} in Aα6, and Asn^{405} in the loop Aβ8-Aα8; see supplemental Fig. 1). All of them are exposed to the solvent, and none are located near the 4F2hc-ED N terminus giving free access of this face of the ectodomain to the plasma membrane surface.

The α-Glycosidase-like Cleft of Human 4F2hc-ED—The catalytic A-domain between the structures of 4F2hc-ED (monoclinic crystal) and oligo-1,6-glucosidase from *Bacillus cereus* (PDB code 1UOK) gives a root mean square standard deviation of 1.96 Å for 260 eq residues (83%). Indeed, the structure of the catalytic A-domain is better preserved than what was anticipated on the basis of the low amino acid sequence identity, in particular for the C-terminal half, starting in Aα4, of the domain (supplemental Fig. 1). The active site of α-amylase family members is highly conserved with key catalytic residues located at the C terminus of the β-strands from the A-domain: a nucleophile (Asp^{199} in 1UOK), a proton donor (Glu^{255}), and a substrate-positioning residue (Asp^{329}) (16). In 4F2hc, this site corresponds to a deep and wide cleft (supplemental Fig. 2*A*), with a distinct shape to that of α-amylases and where only the residue acting as the nucleophile (Asp^{248}) is conserved, although at a slightly different position (supplemental Fig. 1 and Fig. 3*B*). Therefore, the structure indicates that despite its general similarity to α-amylases, 4F2hc is not likely to have α-glycosidase activity. In fact, a detailed screening using D-glucose, D-galactose, or D-mannose derivatives of 4-methylumbelliferone as substrates failed to detect α-glycosidase activity (supplemental Fig. 2*C*).

Zinc Binding and Crystal Homodimer—The two 4F2hc-ED subunits found in the asymmetric unit of the orthorhombic crystal are related by a local 2-fold symmetry with the axis running almost parallel to the c crystal cell edge (Fig. 2*A*). Using x-ray fluorescence spectroscopy (data not shown), a high electron density peak at the interface of the two subunits forming the homodimer was found to correspond to a Zn^{2+} atom (Fig. 2, *A*–*C*). This metal ion sits on the local 2-fold axis and presents a tetrahedral coordination with three residues from the first subunit (Asp^{439} and His^{441}, both in Cβ1, and His^{455} in Cβ2) and only one (His^{441}) from the second subunit (Fig. 2, *B* and *C*). Therefore, coordination of Zn^{2+} breaks the homodimer symmetry precisely in the vicinity of the local 2-fold axis. The unexpected binding of Zn^{2+}, a trace metal not added during purification or crystallization procedures, suggests a high affinity (picomolar range) for this ion. In the 4F2hc-ED subunit determined in the monoclinic crystal, the side chains of Asp^{439}, His^{441}, and His^{455} are exposed to the solvent, without participating in interactions with other protein subunits or in metal coordination (Fig. 2*D*). The homodimer presents a contact surface on each subunit of ~1200 Å with 10 hydrogen bonds and a salt bridge between the two subunits.

Homodimerization of Human 4F2hc in Cultured Cells—To check whether human 4F2hc homodimerizes *in vivo*, HeLa cells were co-transfected with two tagged versions of human 4F2hc (see supplemental Materials and Methods) as follows: 4F2hc-HA (HA tag at the C terminus) and His-4F2hc (six His tag at the N terminus) (Fig. 3*A*). Low molecular weight bands compatible with 4F2hc monomers (85–95 kDa) and high molecular weight bands (up to ~200 kDa) compatible with 4F2hc homodimers were detected with both tags in nonreduc-

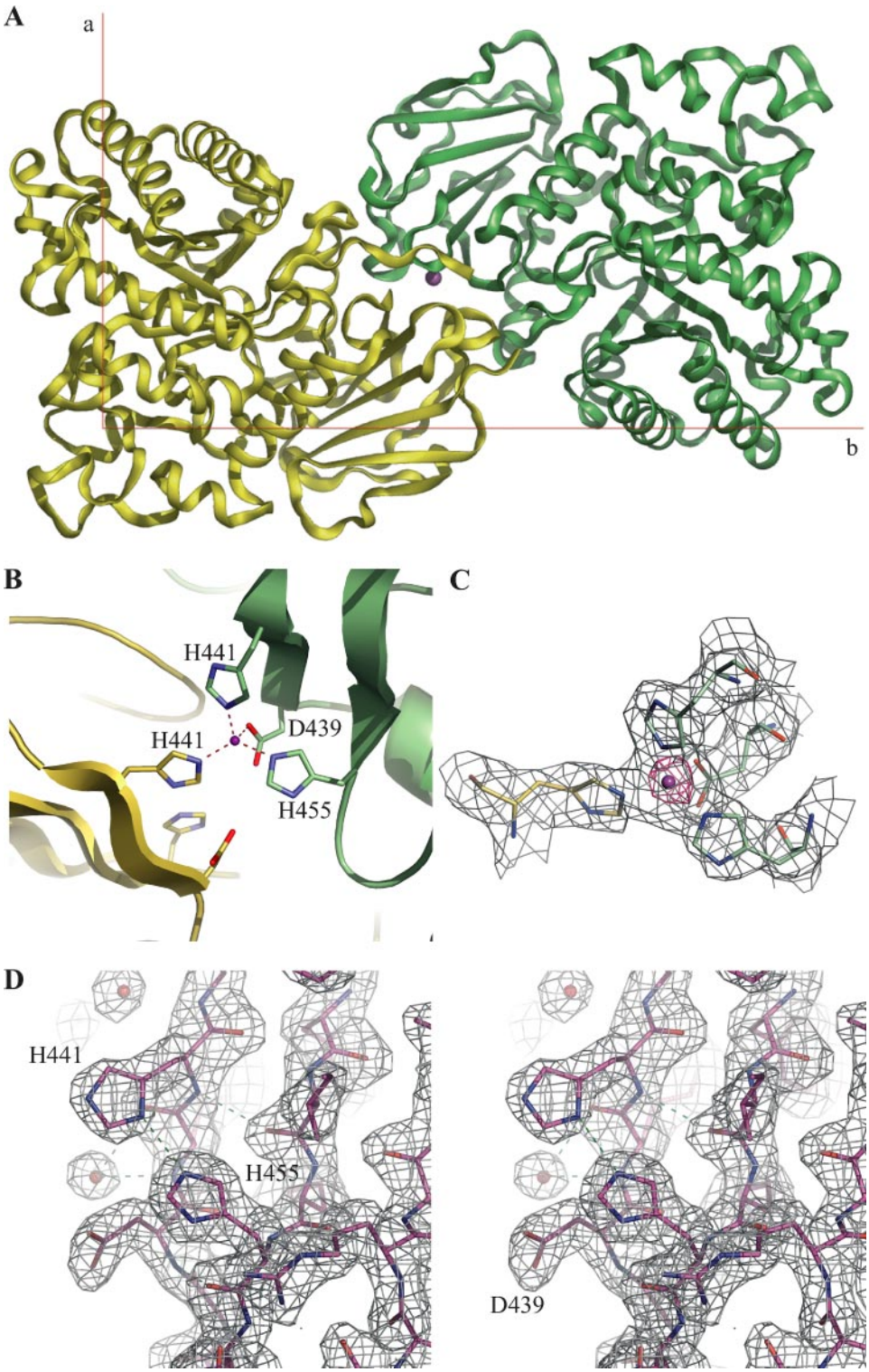

FIGURE 2. **Homodimer of 4F2hc ectodomain.** *A,* ribbons of the two molecules (chains A and B in *green* and *yellow*, respectively) of 4F2hc-ED in the asymmetric unit of the orthorhombic crystal (PDB code 2DH3) with a zinc atom (*purple sphere*) in the interface zone. The homodimer symmetry axis is parallel to crystallographic axis c. *B,* schematic representation of the homodimer interface and tetrahedral coordination of zinc atom. *C,* detail of 2.8 Å 2($F_o - F_c$) density map (*gray* $\sigma = 1$, *pink* $\sigma = 6$) of zinc-coordinated residues. *D,* stereo view of 2.1 Å density map ($\sigma = 1$) for the same residues in the monoclinic crystal where no density for the metal is present.

ing conditions. After His affinity purification, an HA-immunodetected high molecular weight band (170–185 kDa) was observed only in cells co-transfected with both 4F2hc-tagged versions. This indicates the formation of 4F2hc homodimers. These homodimers (*D*) were abolished in reducing conditions (Fig. 3*B*), where only monomers (*M*) and proteolytic fragments (*P*) were visible (Fig. 3*B*; and see supplemental Fig. 4 legend). Human 4F2hc expressed in CHO-K1 cells or in *Xenopus* oocytes also showed DTT-sensitive bands with SDS-PAGE mobility compatible with the formation of homodimers (supplemental Fig. 3). In contrast to HeLa cells (where we have not been able to visualize heterodimers), a band corresponding to the complex of 4F2hc and light subunits (~130 kDa) was detected in CHO-K1 cells expressing human 4F2hc and in oocytes co-expressing human 4F2hc and a tagged version of the light subunit xCT (myc-xCT) (supplemental Fig. 3). These results demonstrate that overexpression of human 4F2hc in cultured cells results in the formation of DTT-sensitive 4F2hc homodimers.

Human 4F2hc contains two Cys residues. Cys^{330} has a lateral side chain that is not accessible to the surface (located just before Aβ7 in the A-domain) and is not expected to be involved in any protein-protein disulfide bridge. Cys^{109} is the residue intervening in the disulfide bridge with 4F2hc-associated light chains (37). Mutation C109S (see supplemental Materials and Methods) abolished the presence of 4F2hc homodimers in SDS-PAGE (Fig. 3*B*). In contrast, mutations that eliminate the Zn^{2+} coordination patch identified in the crystal 4F2hc-ED homodimer (the triple mutant D439A, H441A, and H455A; see supplemental Materials and Methods) did not abolish homodimerization of 4F2hc *in vivo* (Fig. 3*B*). Similar results pointing to the formation of a homodimer of 4F2hc linked by a disulfide bridge through residue Cys^{109} and independent of Zn^{2+} coordination were obtained in oocytes expressing human 4F2hc (supplemental Fig. 3*B*). Interestingly, mutation C109S did not abolish 4F2hc homodimer formation. Thus, 4F2hc monomers were HA-immunodetected after His affinity purification of solubilized material from cell expressing C109S 4F2hc-HA and His-4F2hc (Fig. 3*A*). This co-purification was specific because no 4F2hc-HA signal was detected in His affin-

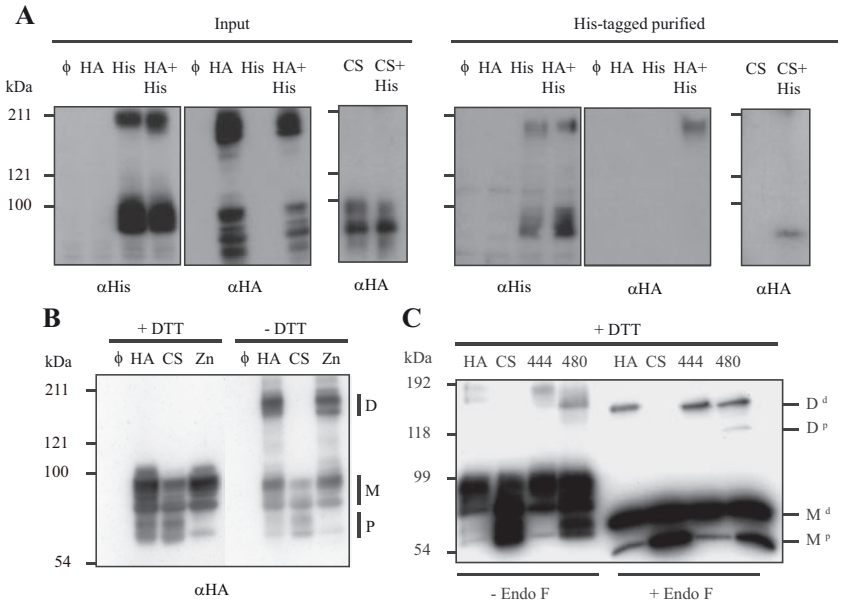

FIGURE 3. **4F2hc homodimerizes in HeLa cells.** *A,* empty pCDNA3.1 vector (*ϕ*), 4F2hc-HA (*HA*), 4F2hc-HA C109S (*CS*), and His-4F2hc (*His*) were transfected alone or in combination (*HA+His*; *CS+His*) in HeLa cells. Proteins were visualized with antibodies anti-His (*αHis*) and −HA (*αHA*) tags before (*Input*) and after Ni-NTA-agarose bead purification. *B,* transient transfection with C-terminal HA-tagged 4F2hc (*HA*) in HeLa cells resulted in the formation of DTT-dependent duplex of bands with high molecular weight compatible with 4F2hc homodimers (*D*). In reducing conditions (*+DTT*), 4F2hc-HA appeared as duplex of bands of low molecular weight, compatible with the size of 4F2hc monomers (*M*) and proteolytic fragments (*P*). Empty pCDNA3.1 vector (*ϕ*) was used as a negative control. Mutation of Cys^{109} to Ser (4F2hc-HA C109S; *CS*) abolished the formation of disulfide bridge-linked homodimers, whereas disruption of the Zn^{2+} coordination patch by mutating all Asp^{439}, His^{441}, and His^{455} to Ala (4F2hc-HA D439A/H441A/H455A; *Zn*) had no effect on the formation of these homodimers. *C,* cross-linking of human 4F2hc homodimers. Intact HeLa cells expressing different versions of human 4F2hc-HA (wild type, *HA*; C109S, *CS*; C109S/S444C, *444*; C109S/S480C, *480*) were treated with the sulfhydryl cross-linker $BM[PEO]_2$ and processed for reducing Western blot. Anti-HA antibody revealed, before Endo F treatment (see supplemental Materials and Methods), glycosylated homodimers (165–180 kDa), monomers (85–95 kDa), and proteolytic fragments (65–75 kDa), and revealed, after Endo F digestion, deglycosylated homodimers (D^d, ~140 kDa), proteolyzed homodimers (D^p, ~115 kDa), monomers (M^d, ~70 kDa), and proteolyzed monomers (M^p, ~55 kDa).

ity-purified extracts from cells expressing C109S 4F2hc-HA alone (Fig. 3*A*). This indicates the tendency to homodimerize of 4F2hc besides disulfide bridge formation.

Human 4F2hc homodimers are formed in the endoplasmic reticulum (ER) as demonstrated by its sensitivity to endo H treatment (supplemental Fig. 4). Surface biotin labeling revealed expression of 4F2hc-HA monomers and homodimers at the plasma membrane, whereas no labeling was observed for an ER marker (BiP) (supplemental Fig. 5).

Confirmation of the 4F2hc Homodimer Architecture in Cultured Cells—The different contribution of Zn^{2+} coordination to homodimerization of 4F2hc in the crystal and *in vivo* raises doubts as to whether the dimer found in the crystal corresponds to the homodimer structure in the cell. To verify this crucial point, we designed a series of cross-linking experiments (Fig. 3*C*) using $BM[PEO]_2$, a reagent that is membrane-impermeable and noncleavable by reducing agents with the capacity to cross-link thiol groups 3.5–14.7 Å apart (38). $BM[PEO]_2$ cross-linked 4F2hc-HA, but not 4F2hc-HA C109S, into homodimers at the surface of HeLa cells (Fig. 3*C*). This suggests that, as expected (see above), Cys^{109} is a target for the cross-linker. Serines 444 and 480 are located in the C-domain between the secondary structures Cβ1 and Cβ2, and Cβ4 and Cβ5, respectively (supplemental Fig. 1), and, on the basis of the crystal homodimer structure, are at a reasonable distance (around 14 Å) to be cross-linked by $BM[PEO]_2$ if mutated to Cys. Interestingly, the reagent cross-linked the double mutants 4F2hc-HA C109S/S444C and 4F2hc-HA C109S/S480C (see supplemental Materials and Methods) into a complex with the SDS-PAGE mobility of 4F2hc-HA homodimers (Fig. 3*C*). These results strongly support the notion that the ectodomains of the 4F2hc homodimer *in vivo* and in the orthorhombic crystal share similar architecture.

Modeling of 4F2hc-ED Homodimers—This modeling was performed to further discard the need of Zn^{2+} coordination for 4F2hc-ED homodimerization. Optimal desolvation area analysis (34) shows that the human 4F2hc-ED is almost absent of patches of low desolvation energy at the surface (data not shown), which suggests that homodimerization is guided by shape and electrostatic complementarities rather than by the hydrophobic effect. Protein-protein docking simulations were performed in the absence of Zn^{2+} coordination by taking two copies of the monomeric structure (PDB code 2DH2) of the protein as ligand and host. No restriction was made to enforce crystal-like packing. The docking solution ranked in position 2 by Pydock was very close to the pseudo-dimer x-ray structure (PDB code 2DH3) (supplemental Table 1 and supplemental Fig. 6), as well other top scored solutions. A final test was performed to check the possibility of alternative structures for the homodimer. For this purpose, the best 500 energy solutions were further filtered by the following criteria: 1) symmetry in the homodimer and distance restrictions for 2) cross-linking experiments and 3) Cys^{109} disulfide bridge formation. These filters recover the information obtained from *in vivo* experiments but do not bias "*per se*" the structure toward the crystal. Application of these filters yielded 11 solutions, 7 of which clustered (supplemental Table 1) in a consensus structure close to the crystal solution (solution ranked 2 is shown in Fig. 4, *B* and *C*). These calculations indicate that the dimer found in the crystal is a true conformation even in the absence of Zn^{2+} coordination. In all, the crystal structure, optimal desolvation area analysis, and docking simulations revealed electrostatic interactions as the driving force for homodimerization.

The Surface Charge Distribution in Monomeric and Dimeric 4F2hc-ED—Electrostatic analysis showed that charged residues at the surface of 4F2hc-ED generate a macromolecular dipole: predominant negatively charged residues on top (face at the C termini of the β-strands of the A-domain) and lateral sides, and predominant positively charge residues on the bottom side (face at the N termini of the β-strands of the A-domain and

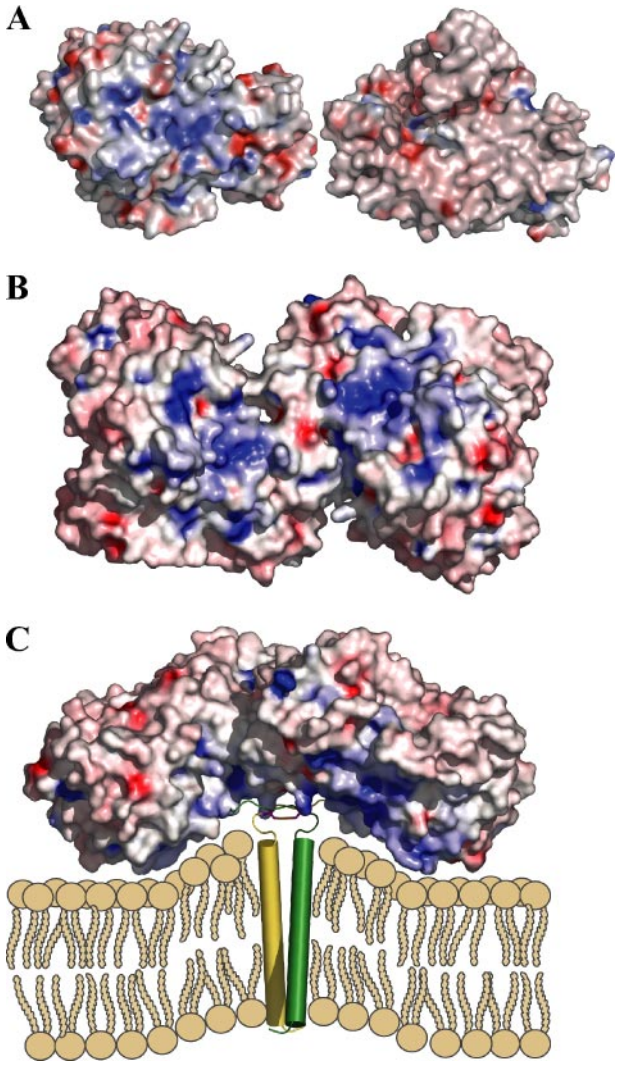

FIGURE 4. **Electrostatic surfaces of 4F2hc-ED homodimer support a model for plasma membrane interaction.** *A,* electrostatic surface of monomer in the monoclinic structure (2DH2) has a dipolar distribution of charges with a positive patch in the N-terminal region (*left*) and negative surface residues in the other sites of the molecule (*right*). *B,* electrostatic surface of N-terminal region of the homodimer from computational docking experiments. *C,* model of 4F2hc homodimer interacting with membrane phospholipids. The positive face of the homodimer has a concave surface and 4F2hc-ED monomer is a rigid structure, as revealed by molecular dynamics analysis and circular dichroism (supplemental Fig. 8). Therefore, two possibilities could be envisaged for the interaction of the ectodomain with the membrane. Either the ectodomain homodimer flattens to adapt to the membrane or deforms the phospholipid bilayer (shown in the figure), as it has been demonstrated for BAR domain homodimers (54).

where the N terminus of the ectodomain is located) (Fig. 4*A*). This dipolar distribution is maintained in the homodimer of 4F2hc-ED, both in the orthorhombic crystal structure (PDB code 2DH3) and in the best solution of the cluster identified from virtual docking (Fig. 4*B*). The large positive patches and their well defined arrangement suggest that they might trigger the interaction of the protein with the plasma membrane.

DISCUSSION

This study provides the first crystal structure of a component of HATs. We previously attempted to model this ectodomain on the base of α-amylases homologous structures without succeeding (1). Once we have solved the structure of 4F2hc-ED, the results are comparable with other structures from α-amylase family. Despite the structural similarities found, the putative active site of 4F2hc presents major differences with respect to these enzymes. Accordingly, purified 4F2hc-ED showed no α-glycosidase activity for glucose-, galactose-, and mannose-intervening substrates. In contrast, the derived structural model of the ectodomain of human rBAT suggests the presence of the main catalytic features found in α-amylases, including a B-domain, and consequently the conservation of glycosyl hydrolase activity (supplemental Fig. 1).

The lack of this type of activity for 4F2hc-ED might indicate that this ectodomain still retains glycosidase-like binding properties. Other glycosidase-derived proteins such as the cytokines Ym1/2 (39, 40) and the ER degradation enhancing α-mannosidase I-like protein (41) have lectin activity. Unfortunately, a massive analysis performed using the Glycomics glycan chip (containing more than 260 glycans) failed to find any interacting glycan (data not shown; see supplemental Materials and Methods). Possible binding of proteins or glycoproteins to the wide cleft of 4F2hc-ED is supported by the observation that some glycosidase inhibitors bind at the catalytic cleft and have Ig-like structures (*e.g.* Tendamistat (42)). Several proteins with this type of structure (*e.g.* galectin-3, ICAM-1, CD-147, and CEA-CAM-1) have been proposed to interact with 4F2hc-ED (12, 15, 43–45).

In this study we have demonstrated the formation of 4F2hc homodimers linked by a disulfide bridge between Cys^{109} residues in several cell types expressing the human protein. Although 4F2hc homodimers have not been described previously, interpreting published data DTT-sensitive 4F2hc homodimer-compatible bands seem to be present in oocytes and COS cells expressing human 4F2hc and in human T lymphoblastoid cells (46–48). Homodimerization of 4F2hc could be facilitated by overexpression of the protein, but the tendency of the protein to dimerize is supported by the fact that the interconnecting disulfide bridge is not essential. The 4F2hc-ED homodimer found in the orthorhombic crystal most probably reflects the principal features of the homodimerization of 4F2hc *in vivo*, as only the putative *N*-glycosylation site Asn^{323} is near the homodimerization surface, and the crystal homodimer is compatible with the restrictions imposed both by cross-linking experiments and by formation of the Cys^{109}-intervening disulfide bridge. Most probably the interaction of the ectodomains in 4F2hc homodimers are of low affinity; this dimerization was observed only in one type of crystals, and gel filtration of 4F2hc-ED revealed only the monomeric form (data not shown). This suggests that other parts of the protein (transmembrane domain and intracellular N terminus) trigger homodimerization of 4F2hc.

Despite the unexpected presence of Zn^{2+} at the interface of the crystal homodimer, the coordination of this metal does not appear to be required for 4F2hc homodimerization *in vivo*: (i) the Zn^{2+} coordination is not necessary for homodimerization of 4F2hc expressed in cells; (ii) the residues involved are not conserved in mammals; and (iii) computational 4F2hc-4F2hc docking experiments yielded a cluster of solutions very similar to the crystal homodimer (without the Zn^{2+} coordination), compatible with the binary symmetry, the Cys^{109} disulfide

bridge formation, and our cross-linking results. Zn^{2+} coordination does not seem to play a role in the heterodimers. Mutation of the coordinating residues did not affect functional interaction of 4F2hc with light subunit xCT, even in the absence of the Cys^{109}-intervening disulfide bridge (supplemental Fig. 7). Thus, Zn^{2+} coordination in human 4F2hc could be relevant for other protein interactions. Indeed, a very similar Zn^{2+} coordination arrangement has been described in the superantigen *Staphylococcus aureus* enterotoxin A for high affinity interaction with major histocompatibility complex class II molecules (49).

Overexpression of 4F2hc in cells increases β1 integrin signaling (*i.e.* phosphatidylinositol 3-hydroxykinase, focal adhesion kinase, and Akt), and this leads to cell transformation (50) and tumorigenesis in mice (10). The previously accepted view was that 4F2hc occurs in cells only as heterodimers (48). Here we show that overexpression of 4F2hc results in the presence of monomers and homodimers in the cell surface, which might have a role on the functions of 4F2hc in these conditions. In this sense, C109S mutation resulted in a maturation defect (*i.e.* lesser acquisition of complex *N*-glycosylation) of 4F2hc (Fig. 3), suggesting that homodimerization helps maturation and trafficking of 4F2hc. Thus, the Endo H-resistant form of C109S 4F2hc is underexpressed in HeLa cells (19 ± 4% of total expressed 4F2hc *versus* 45 ± 2% for wild-type 4F2hc; Student's *t* test, $p < 0.001$ for $n = 6$ independent transfections). Interestingly, C109S 4F2hc shows neither association with β1 integrin (51) nor cell transformation activity in cells overexpressing the protein (52). This correlation supports a role of 4F2hc homodimers in cell transformation.

Our results allow proposing a model for the disposition of 4F2hc homodimer in the membrane (Fig. 4*B*). No hydrophobic exposed patches were found in the 4F2hc-ED surface. Thus, major hydrophobic interaction of 4F2hc with the membrane will be due to the highly hydrophobic transmembrane domain. The surface of 4F2hc-ED homodimer displays a marked polarized charge distribution with a positive surface in the N terminus toward the Cys^{109} disulfide bridge and the transmembrane domain. This observation strongly suggests an electrostatic interaction of 4F2hc-ED with the phospholipid polar heads of the plasma membrane, characteristic of several peripheral and integral membrane proteins (53). This model might also provide clues about the arrangement of 4F2hc within the heterodimer in the plasma membrane because 4F2hc homo- and heterodimerization should be competitive processes because residue Cys^{109} participates in the disulfide bridge between monomers (this study) and in the heterodimers (37). In addition, the homodimer architecture suggests that the C-domain has a tendency for protein interaction. The external loops of the 4F2hc-associated light subunits might interact similarly with the C-domain, thereby favoring the docking of 4F2hc-ED onto the membrane. Moreover, the electrostatic nature of the 4F2hc-ED interaction with plasma membrane might facilitate dynamic interaction with their multiple interacting proteins (*e.g.* light chains, β1 integrin complexes, CD147, and galectin-3).

The structure of the 4F2hc ectodomain solved here seriously questions a catalytic role for this domain despite its overall similarities with α-amylases, brings the hypothesis of acting as a receptor for ligands, supports an electrostatic interaction with the plasma membrane, and represents the first step toward the elucidation of the atomic structure of the heteromeric amino acid transporters. Moreover, the homodimerization of 4F2hc introduces a new element to understand the mechanisms involved in the functions of this protein in cell adhesion, cell transformation, and tumorigenesis that need further investigation.

Acknowledgments—We thank Susanna Bial (Institute for Research in Biomedicine and Centro de Investigación Biomédica en Red de Enfermedades Raras, Barcelona) for technical assistance. We also thank Chantal Abergel (CNRS, Marseille) who taught us how to use CaspR, and Tania Yates for English editing of the manuscript. We acknowledge Richard Alvarez and Angela Lee, from the Consortium for functional glycomics, for glycan binding screening.

REFERENCES

1. Chillaron, J., Roca, R., Valencia, A., Zorzano, A., and Palacin, M. (2001) *Am. J. Physiol.* **281,** F995–F1018
2. Tsurudome, M., and Ito, Y. (2000) *Crit. Rev. Immunol.* **20,** 167–196
3. Fenczik, C. A., Sethi, T., Ramos, J. W., Hughes, P. E., and Ginsberg, M. H. (1997) *Nature* **390,** 81–85
4. Torrents, D., Mykkanen, J., Pineda, M., Feliubadalo, L., Estevez, R., de Cid, R., Sanjurjo, P., Zorzano, A., Nunes, V., Huoponen, K., Reinikainen, A., Simell, O., Savontaus, M. L., Aula, P., and Palacin, M. (1999) *Nat. Genet.* **21,** 293–296
5. Borsani, G., Bassi, M. T., Sperandeo, M. P., De Grandi, A., Buoninconti, A., Riboni, M., Manzoni, M., Incerti, B., Pepe, A., Andria, G., Ballabio, A., and Sebastio, G. (1999) *Nat. Genet.* **21,** 297–301
6. Kaleeba, J. A., and Berger, E. A. (2006) *Science* **311,** 1921–1924
7. Bellone, G., Alloatti, G., Levi, R., Geuna, M., Tetta, C., Peruzzi, L., Letarte, M., and Malavasi, F. (1989) *Eur. J. Immunol.* **19,** 1–8
8. Garber, M. E., Troyanskaya, O. G., Schluens, K., Petersen, S., Thaesler, Z., Pacyna-Gengelbach, M., van de Rijn, M., Rosen, G. D., Perou, C. M., Whyte, R. I., Altman, R. B., Brown, P. O., Botstein, D., and Petersen, I. (2001) *Proc. Natl. Acad. Sci. U. S. A.* **98,** 13784–13789
9. Yoon, J. H., Kim, Y. B., Kanai, Y., Endou, H., and Kim, D. K. (2003) *Anticancer Res.* **23,** 3877–3881
10. Hara, K., Kudoh, H., Enomoto, T., Hashimoto, Y., and Masuko, T. (2000) *Oncogene* **19,** 6209–6215
11. Feral, C. C., Nishiya, N., Fenczik, C. A., Stuhlmann, H., Slepak, M., and Ginsberg, M. H. (2005) *Proc. Natl. Acad. Sci. U. S. A.* **102,** 355–360
12. Xu, D., and Hemler, M. E. (2005) *Mol. Cell. Proteomics* **4,** 1061–1071
13. Broer, A., Friedrich, B., Wagner, C. A., Fillon, S., Ganapathy, V., Lang, F., and Broer, S. (2001) *Biochem. J.* **355,** 725–731
14. Fenczik, C. A., Zent, R., Dellos, M., Calderwood, D. A., Satriano, J., Kelly, C., and Ginsberg, M. H. (2001) *J. Biol. Chem.* **276,** 8746–8752
15. Dalton, P., Christian, H. C., Redman, C. W., Sargent, I. L., and Boyd, C. A. (2007) *FEBS J.* **274,** 2715–2727
16. Janecek, S. (1997) *Prog. Biophys. Mol. Biol.* **67,** 67–97
17. Chillaron, J., Estevez, R., Mora, C., Wagner, C. A., Suessbrich, H., Lang, F., Gelpi, J. L., Testar, X., Busch, A. E., Zorzano, A., and Palacin, M. (1996) *J. Biol. Chem.* **271,** 17761–17770
18. Claude, J. B., Suhre, K., Notredame, C., Claverie, J. M., and Abergel, C. (2004) *Nucleic Acids Res.* **32,** 606–609
19. Vagin, A., and Teplyakov, A. (1997) *J. Appl. Crystallogr.* **30,** 1022–1025
20. Murshudov, G. N., Vagin, A. A., and Dodson, E. J. (1997) *Acta Crystallogr. Sect. D. Biol. Crystallogr.* **53,** 240–255
21. Navaza, J. (2001) *Acta Crystallogr. Sect. D. Biol. Crystallogr.* **57,** 1367–1372
22. Cowtan, K. (1994) *Joint CCP4 and ESF-EACBM Newsletter on Protein Crystallography* **31,** 34–38
23. Jones, T. A., Zou, J. Y., Cowan, S. W., and Kjeldgaard, M. (1991) *Acta*

Crystallogr. Sect. A **47,** 110–119
24. Laskowski, R. A., Moss, D. S., and Thornton, J. M. (1993) *J. Mol. Biol.* **231,** 1049–1067
25. O'Sullivan, O., Suhre, K., Abergel, C., Higgins, D. G., and Notredame, C. (2004) *J. Mol. Biol.* **340,** 385–395
26. Gouet, P., Robert, X., and Courcelle, E. (2003) *Nucleic Acids Res.* **31,** 3320–3323
27. Binkowski, T. A., Naghibzadeh, S., and Liang, J. (2003) *Nucleic Acids Res.* **31,** 3352–3355
28. Nicholls, A., Sharp, K. A., and Honig, B. (1991) *Proteins* **11,** 281–296
29. DeLano, W. L. (2002) *The PyMOL Molecular Graphics System,* Version 0.99rc6, DeLano Scientific, San Carlos, CA
30. Cornell, W. D., Cieplak, P., Bayly, C. I., Gould, I. R., Merz, K. M., Ferguson, D. M., Spellmeyer, D. C., Fox, T., Caldwell, J. W., and Kollman, P. A. (1996) *J. Am. Chem. Soc.* **118,** 2309
31. Kale, L., Skeel, R., Bhandarkar, M., Brunner, R., Gursoy, A., Krawetz, N., Phillips, J., Shinozaki, A., Varadarajan, K., and Schulten, K. (1999) *J. Comput. Physics* **151,** 283–312
32. Phillips, J. C., Braun, R., Wang, W., Gumbart, J., Tajkhorshid, E., Villa, E., Chipot, C., Skeel, R. D., Kale, L., and Schulten, K. (2005) *J. Comput. Chem.* **26,** 1781–1802
33. Rueda, M., Ferrer-Costa, C., Meyer, T., Perez, A., Camps, J., Hospital, A., Gelpi, J. L., and Orozco, M. (2007) *Proc. Natl. Acad. Sci. U. S. A.* **104,** 796–801
34. Fernandez-Recio, J., Totrov, M., Skorodumov, C., and Abagyan, R. (2005) *Proteins* **58,** 134–143
35. Man-Kuang Cheng, T., Blundell, T. L., and Fernandez-Recio, J. (2007) *Proteins* **68,** 503–515
36. Gabb, H. A., Jackson, R. M., and Sternberg, M. J. (1997) *J. Mol. Biol.* **272,** 106–120
37. Pfeiffer, R., Spindler, B., Loffing, J., Skelly, P. J., Shoemaker, C. B., and Verrey, F. (1998) *FEBS Lett.* **439,** 157–162
38. Green, N. S., Reisler, E., and Houk, K. N. (2001) *Protein Sci.* **10,** 1293–1304
39. Chang, N. C., Hung, S. I., Hwa, K. Y., Kato, I., Chen, J. E., Liu, C. H., and Chang, A. C. (2001) *J. Biol. Chem.* **276,** 17497–17506
40. Tsai, M. L., Liaw, S. H., and Chang, N. C. (2004) *J. Struct. Biol.* **148,** 290–296
41. Hosokawa, N., Wada, I., Natsuka, Y., and Nagata, K. (2006) *Genes Cells* **11,** 465–476
42. Wiegand, G., Epp, O., and Huber, R. (1995) *J. Mol. Biol.* **247,** 99–110
43. Dong, S., and Hughes, R. C. (1997) *Glycoconj. J.* **14,** 267–274
44. Liu, X., Charrier, L., Gewirtz, A., Sitaraman, S., and Merlin, D. (2003) *J. Biol. Chem.* **278,** 23672–23677
45. Kakugawa, K., Hattori, M., Beauchemin, N., and Minato, N. (2003) *FEBS Lett.* **552,** 184–188
46. Hemler, M. E., and Strominger, J. L. (1982) *J. Immunol.* **129,** 623–628
47. Torrents, D., Estevez, R., Pineda, M., Fernandez, E., Lloberas, J., Shi, Y. B., Zorzano, A., and Palacin, M. (1998) *J. Biol. Chem.* **273,** 32437–32445
48. Nakamura, E., Sato, M., Yang, H., Miyagawa, F., Harasaki, M., Tomita, K., Matsuoka, S., Noma, A., Iwai, K., and Minato, N. (1999) *J. Biol. Chem.* **274,** 3009–3016
49. Sundstrom, M., Hallen, D., Svensson, A., Schad, E., Dohlsten, M., and Abrahmsen, L. (1996) *J. Biol. Chem.* **271,** 32212–32216
50. Henderson, N. C., Collis, E. A., Mackinnon, A. C., Simpson, K. J., Haslett, C., Zent, R., Ginsberg, M., and Sethi, T. (2004) *J. Biol. Chem.* **279,** 54731–54741
51. Kolesnikova, T. V., Mannion, B. A., Berditchevski, F., and Hemler, M. E. (2001) *BMC Biochem.* **2,** 10
52. Shishido, T., Uno, S., Kamohara, M., Tsuneoka-Suzuki, T., Hashimoto, Y., Enomoto, T., and Masuko, T. (2000) *Int. J. Cancer* **87,** 311–316
53. Mulgrew-Nesbitt, A., Diraviyam, K., Wang, J., Singh, S., Murray, P., Li, Z., Rogers, L., Mirkovic, N., and Murray, D. (2006) *Biochim. Biophys. Acta* **1761,** 812–826
54. Blood, P. D., and Voth, G. A. (2006) *Proc. Natl. Acad. Sci. U. S. A.* **103,** 15068–15072